J Low Temp Phys (2008) 150: 525–535
DOI 10.1007/s10909-007-9587-3

Vibrating Quartz Fork—A Tool for Cryogenic Helium Research

M. Blažková · M. Človečko · V.B. Eltsov · E. Gažo · R. de Graaf · J.J. Hosio · M. Krusius · D. Schmoranzer · W. Schoepe · L. Skrbek · P. Skyba · R.E. Solntsev · W.F. Vinen

Received: 18 July 2007 / Accepted: 17 October 2007 / Published online: 30 November 2007

Abstract Oscillating objects such as discs, piles of discs, spheres, grids and wires have been widely used in cryogenic fluid dynamics and in quantum fluids research since the discovery of superfluidity. A new addition are quartz tuning forks, commercially available frequency standards. We review their use as thermometers, pressure- and viscometers as well as their potential as generators and detectors of cavitation and turbulence in viscous and superfluid He liquids.

Keywords Low temperature instrumentation and new techniques · Normal 3He · Superfluid 3He · Superfluid 4He · Turbulence

PACS 07.10.-h · 47.37.+q · 67.57.De

M. Blažková
Institute of Physics ASCR, v.v.i., Na Slovance 2, 182 21 Prague, Czech Republic

M. Človečko · E. Gažo · P. Skyba
Center of Low Temperature Physics, Institute of Experimental Physics, Watsonova 47, 04 001 Kosice, Slovakia

V.B. Eltsov · R. de Graaf · J.J. Hosio · M. Krusius · R.E. Solntsev
Low Temperature Laboratory, Helsinki University of Technology, 02015-TKK, Helsinki, Finland

D. Schmoranzer · L. Skrbek (✉)
Faculty of Mathematics and Physics, Charles University, V Holešovičkách 2, 180 00 Prague, Czech Republic
e-mail: skrbek@fzu.cz

W. Schoepe
Fakultät für Physik, Universität Regensburg, 93040 Regensburg, Germany

W.F. Vinen
School of Physics and Astronomy, University of Birmingham, Birmingham B15 2TT, UK

1 Introduction

Various types of oscillating structures have been important for probing the hydrodynamic properties of quantum fluids since the discovery of superfluidity. The Andronikashvili experiment [1–3], the basis for the two fluid model, was a measurement of the torsional oscillations of a pile of closely spaced discs and was the first direct determination of the densities of the normal (ρ_n) and superfluid (ρ_s) fractions in He II, while measurements with oscillating discs, spheres, capillary flow, or U-tube oscillations have been employed to display various "critical velocities" above which the ideal two-fluid picture did not hold. The reason for using various oscillating structures is obvious—in a cryostat it is technically simpler to generate flow with oscillating objects rather than by some more complicated external drive, as would be needed, e.g., for pipe flow.

In more recent times the use of vibrating wire loops has regained importance. Originally a fine conducting wire stretched along the axis of a cylindrical rotating container was used by Vinen [4] as a sensor to prove quantization of vorticity in He II. Today fine superconducting vibrating wires, usually in the form of a half-loop a few mm in diameter, are the most widely used resonators. They have been used for investigating the nucleation of quantized vorticity in He II (e.g. [5–7]) and in ^{3}He-B (e.g. [8, 9]), as thermometers, pressure- and viscometers in ^{4}He, ^{3}He and ^{4}He-^{3}He mixtures over a wide temperature range, even down to microkelvin temperatures [10]. They are driven by the Lorentz force from a small ac current bias in an applied magnetic field.

The quartz tuning fork is a piezoelectric resonator (Fig. 1), which is mass produced as frequency standard for digital watches and which now has found a large number of other applications [11, 12]. It is cheap, sensitive, robust, and easy to install and to use. Only two wires are needed to drive and readout a fork as sensor; no magnetic field is needed. In fact, the fork is quite insensitive to magnetic fields and becomes thus useful as a field-independent sensor in measurements as a function of magnetic field. A relatively simple electronic scheme composed of a digital oscillator and a lock-in amplifier (see, e.g. Ref. [13]) is used for detecting its resonant response over seven orders of magnitude of the driving force in both viscous and quantum fluids. Because of these many convenient features the fork is becoming an indispensable monitoring tool in the He sample cell, starting from sensitive monitoring of pressures during flushing, evacuation, and filling of complicated cell structures, and continuing all the way to liquid ^{3}He thermometry at sub-millikelvin temperatures in the ballistic regime of quasiparticle excitations. This has provided a strong motive to explore the applicability of the quartz tuning fork further, especially as a generator and sensor of vortices in the He superfluids.

The quartz tuning fork comes inside a vacuum-tight metal can and when cooled, its resonant frequency f_0 decreases and the Q value increases. At LHe temperatures the reduction in resonant frequency from the room-temperature value (typically 2^{15} Hz) is about 70 Hz and the Q value approaches 10^6. If the can is removed, the bare fork in vacuum behaves in a similar manner: The reduction in the resonant frequency remains the same while the Q value is typically lower than for the fork inside its original can. However, the Q value varies from one fork to another, typically in the range from

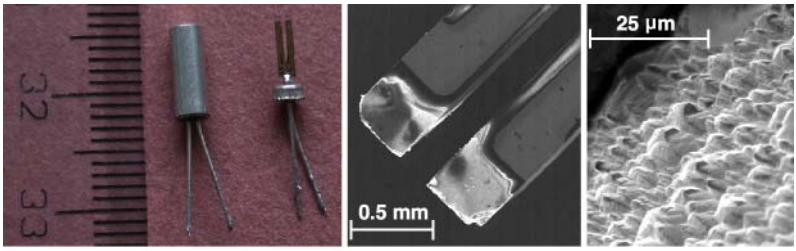

Fig. 1 (Color online) Photographs of quartz tuning forks, both with the fork in its original can and with the can removed (*left*). The micrographs show the ends of its prongs (*middle*) and the characteristic surface roughness (*right*)

$2 \cdot 10^4$ to $5 \cdot 10^5$. To maintain high Q values, care should be used not to strain the quartz while cutting away the can, when bending the leads, or while replacing them with non-magnetic wires in magnetic applications. In this short review we briefly summarize earlier work on their use in He experiments [13–16] and describe some new results, which further strengthen their potential as a multi-purpose cryogenic sensor.

2 Tuning Fork as Sensor in Linear Regime

At low amplitude in the linear drive regime the quartz tuning fork is used as secondary thermometer, pressure gauge, viscometer, or flowmeter in measurements on normal and superfluid ^{4}He and ^{3}He. Its advantage is that with a single sensor in one and the same setup all these different types of tasks can be performed from room temperature down to the lowest temperature. In the linear regime the flow around the fork is laminar[1] and its response behaves in good accordance with hydrodynamic models [13]. Different tuning forks, even if they originate from the same manufacturing batch, do not appear to obey exactly the same calibration in LHe temperature measurements [13]. However, by preselecting the forks according to their Q values at some temperature in the LHe range in vacuum, similar behavior can be expected.

In superfluid ^{3}He work, for instance, the fork is a most useful secondary thermometer. It requires less work and know how to implement and to operate than any other of the current methods for thermometry. It can be used as thermometer from the normal state down to the very lowest temperatures with good sensitivity and seems to provide reproducible readings even in the anisotropic A phase. At temperatures below $0.3\,T_c$ its temperature dependence can be extrapolated using $Q = f_0/\Delta f \propto \exp(\Delta/k_B T)$, where $\Delta(T, P)$ is the superfluid energy gap. The proportionality factor in this calibration can be fixed at one known temperature.

[1] It appears that the response of the fork depends weakly on the geometry of the surrounding container. This effect is attributed to the existence of steady secondary flow through the action of viscosity in the boundary layer, called "streaming" [17]. As far as we know, this effect has not been taken into account in the analysis of measurements recorded with oscillating objects, most notably with vibrating wires. It might become important in accurate measurements of physical quantities spanning a large range of values.

In principle, also in He I and He II both the resonance frequency and width can be used for thermometry. Owing to the extremely low kinematic viscosity of He I and of the normal component in He II the temperature-induced changes in the response of the fork are small. External interference from other sources, such as flow or solid particles raining on the fork in technical helium, may then become a problem. However, the fact that the fork is sensitive to such features makes it useful for other purposes, as we will see below, but limits its use as thermometer or pressure gauge in technical ^{4}He in an open dewar. For accurate and reproducible readings the fork should be housed in a shielded volume or be used in its original can which is only partly removed. When filling a separate sample cell where a tuning fork is located, the ^{4}He charge should be introduced via a cryotrap and/or a sufficiently fine filter, to avoid particles of air or water, which would float in the liquid and settle on the quartz surface.

3 Tuning Fork as Generator and Detector of Turbulence in ^{4}He

At large drive the prongs of the tuning fork vibrate at high velocities up to 10 m/s. This can be used for different types of studies, including cavitation in He I and He II along the saturated vapor pressure curve and at slightly elevated pressures. Cavitation is observed as a breakdown of the resonance response at a critical velocity, while slowly sweeping the frequency of the drive across resonance [18]. A second application at higher drives is the measurement of turbulence.

3.1 Transition from Laminar to Turbulent Drag in Normal Viscous Fluids

The damping of the tuning fork has been investigated by the Prague group in gaseous ^{4}He at liquid nitrogen temperature at external pressures up to 30 bar and in normal He I liquid [15]. For measurements on classical fluid dynamics He is a remarkable working fluid—a playground where the density and kinematic viscosity can be tuned by orders of magnitude in situ, by changing temperature and pressure in the sample cell. Combined with the large dynamic range of the fork (more than seven decades over which its response to the harmonic drive can be detected), one has an ideal system for studying the transition from laminar to turbulent drag and the scaling of the critical velocity associated with this transition.

From a measurement of the velocity versus the driving force (Fig. 2), it is found that in viscous flow the critical velocity for the crossover from laminar to turbulent drag in the limit $U/\omega \ll \ell \gg \delta$ scales as $U_{\rm cr} \propto \sqrt{\nu\omega}$ over at least two decades of kinematic viscosity ν [15]. Here U is the peak velocity of the fork, ℓ its characteristic size, ω its angular frequency, and $\delta = \sqrt{2\nu/\omega}$ the viscous penetration depth. The validity of this scaling was recently tested further by performing measurements with forks of various sizes and oscillating at different frequencies.[2] The scaling can be explained qualitatively by equating the linear and the turbulent drag forces at $U_{\rm cr}$, using the approach described in Ref. [15].

[2]The data obtained with different forks in liquid and gaseous helium as well as visualizations of dynamically similar flow in water at room temperature using the Baker pH technique will be described elsewhere.

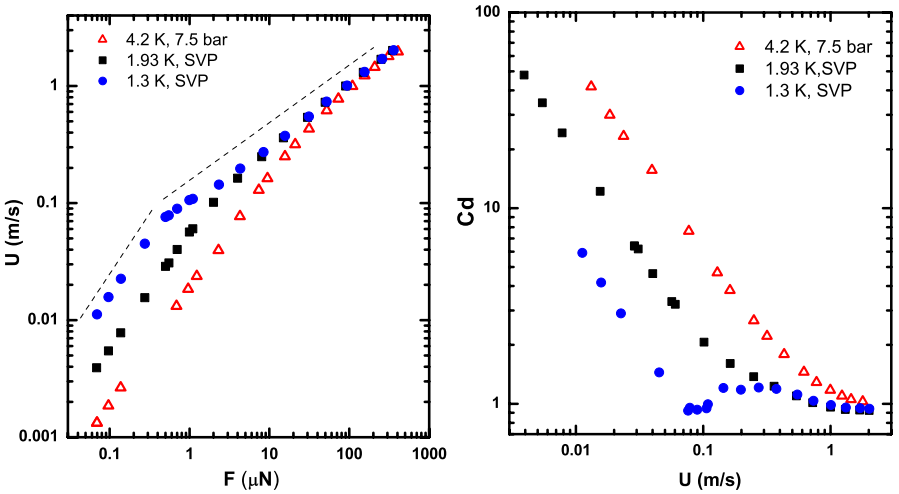

Fig. 2 (Color online) *(Left)* Transition from laminar to turbulent flow in ^{4}He, measured with a tuning fork in He I and He II at three temperatures. At low drive level (in the laminar regime) the velocity is a linear function of the applied drive, while after the crossover to the turbulent regime the driving force is proportional to the square of the velocity. The *dashed lines* indicate the slopes $U \propto F$ and $U \propto \sqrt{F}$. *(Right)* In viscous fluid (He I) the drag coefficient C_d plotted versus velocity tends gradually towards constant value at high velocities in the turbulent regime, while in He II the superfluid fraction causes a sharp transition at a critical velocity U_cr^S

3.2 Transition from Laminar to Turbulent Drag in He II

The analysis has been recently extended from viscous He I to superfluid He II (a preliminary report is Ref. [16]). The left panel of Fig. 2 shows no appreciable qualitative change in the character of the dependence of the velocity versus driving force when crossing T_λ. On decreasing the temperature of He II along the saturated vapor pressure curve further, however, the crossover from laminar to turbulent flow becomes gradually sharper and the character of the curve above the critical velocity changes. This change is seen more clearly in the right panel of Fig. 2, where the drag coefficient C_d is plotted for three different temperatures.[3] C_d is defined from the equation

$$F = \frac{1}{2} C_\mathrm{d} \rho A U^2, \tag{1}$$

where ρ is the fluid density and A is the projected area of one prong of the fork on a plane normal to the bulk flow. For laminar viscous flow the drag is approximately proportional to U, so that $C_\mathrm{d} \sim U^{-1}$. We see that in classical viscous He I, in the vicinity of U_cr, the measured dependence $C_\mathrm{d}(U)$ gradually levels off and C_d acquires

[3]The data shown for He I at 4.2 K have been measured at elevated pressure, as at saturated vapor pressure the fork vibrating at high velocity of order 50 cm/s causes cavitation [18], preventing measurements in the turbulent drag regime up to the highest possible velocities. In He II on the saturated vapor pressure curve cavitation occurs at velocities of order 2 m/s far inside the turbulent regime.

an approximately constant value of order unity. In He II well below T_λ, $C_\mathrm{d}(U)$ behaves differently. It displays the laminar part, where the drag is due to the viscous normal fluid only. Beyond a sharp minimum, $C_\mathrm{d}(U)$ increases again and displays a broad maximum above which it gradually becomes constant as in the classical case.

This behavior of the drag coefficient $C_\mathrm{d}(U)$ can be understood in the framework of the two-fluid model, assuming that the total drag consists of two independent contributions. The normal fraction behaves similar to any classical viscous fluid and causes the leveling off in $C_\mathrm{d}(U)$ at higher velocities (curve at 1.3 K in right panel of Fig. 2). The critical velocity U_cr^N can be determined in analogy with U_cr in He I. The superfluid fraction produces the sharp minimum where the turbulent drag sets in, which is identified as its critical velocity U_cr^S. It was found, at least approximately, to be frequency independent, while $U_\mathrm{cr}^\mathrm{N} \propto \sqrt{\omega}$. Consequently, thanks to the high oscillating frequency of the fork, the two critical velocities appear well separated, which makes this analysis possible.

The transition from laminar to turbulent drag regime has been experimentally studied with a number of different vibrating structures of various shapes (such as wires [6, 7], spheres [19–21], grids [22], and forks [16]) in a range of temperatures down to the zero-temperature limit. The observed critical velocity is often found to depend on the prehistory of vortices in the sample cell (i.e. on the presence of trapped vortices) and in some cases, e.g., for thin vibrating wires [6, 7], it is seen to be frequency dependent. New measurements on the fork response in the low temperature limit are in progress and their detailed theoretical analysis using computer simulations [23] as illustration should clarify these questions further.

4 Tuning Fork and Andreev Reflection in ^{3}He-B

In superfluid ^{3}He-B the quartz tuning fork has been used in different types of measurements on quantized vortices. At present the simplest demonstration of vortex generation and its detection with a tuning fork is to use the signal from Andreev scattering, the reflection of quasiparticle excitations from the superflow fields in a vortex tangle, as has been observed and explained by Fisher et al. for vibrating wire resonators [25]. Andreev reflection has been demonstrated by the Košice group in measurements with a single fork where the quasiparticle excitations are most likely scattered by potential flow around the vibrating legs of the fork. The Helsinki group has used a pair of forks, where one acts as generator of the turbulent vortex tangle and the other as detector of the quasiparticle density.

4.1 Andreev Reflection from Potential Flow Fields

The inset in Fig. 3 (left panel) shows the dependence of the damping force versus velocity of the tuning fork, measured in ^{3}He-B at 245 μK. Up to velocities of about 2 mm/s this dependence appears linear at first sight, without a tendency to saturation, as is usual for vibrating wires [8]. However, a detailed view at very low drives shows that the measured linewidth Δf initially decreases with increasing drive, resulting in a deviation (of up to 10 %) of the damping force from the linear dependence.

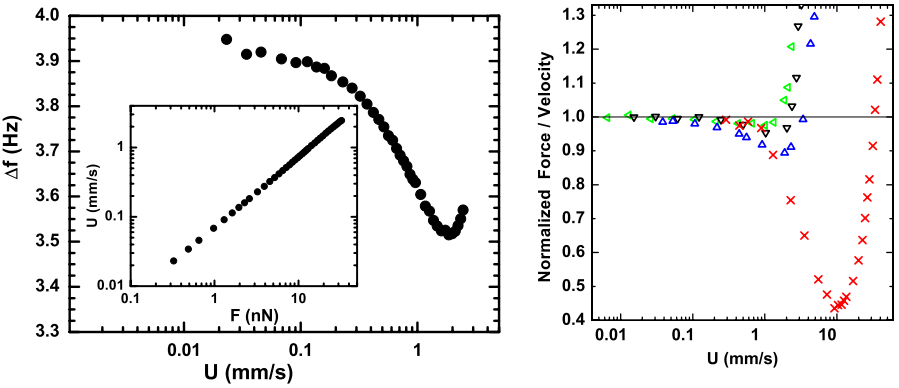

Fig. 3 (Color online) *(Left)* Dependence of the fork width Δf on the fork velocity U, measured at 245 μK and 0.5 bar. The *inset* shows the corresponding force versus velocity dependence. *(Right)* The normalized ratio force/velocity plotted versus velocity shows the departure from unity to lower values owing to Andreev reflection, until other contributions start to interfere. *Triangles pointing left* (*green* online), *down* and *up* (*black* and *blue* online) are measured for the fork at 360 μK, 275 μK and 220 μK. The *crosses* (*red* online) denote the corresponding data for a 13 μm diameter vibrating wire at 220 μK

The motion of an object in ^{3}He-B is damped by the scattering of quasiparticle excitations. A simple model was introduced in Ref. [8], to express the damping force per unit area

$$F_{\mathrm{T}} = p_{\mathrm{F}}\langle n V_{\mathrm{g}}\rangle \left[1 - \exp\left(\frac{-\lambda p_{\mathrm{F}}}{k_{\mathrm{B}}T}U\right)\right], \tag{2}$$

where V_{g} is the group velocity of excitations, p_{F} the Fermi momentum, U the velocity of the object, λ a constant characterizing the velocity field around the object, and $\langle n V_{\mathrm{g}}\rangle = n(p_{\mathrm{F}})k_{\mathrm{B}}T\exp(-\Delta/k_{\mathrm{B}}T)$ represents the quasiparticle flux. Here $n(p_{\mathrm{F}})$ is the density of states in momentum space. The assumption that $p_{\mathrm{F}}U \ll k_{\mathrm{B}}T$ allows us to expand $\exp(-p_{\mathrm{F}}U/k_{\mathrm{B}}T)$ as a Taylor series. Taking into account the first three terms one gets:

$$F_{\mathrm{T}} = n(p_{\mathrm{F}})p_{\mathrm{F}}^2\lambda\exp(-\Delta/k_{\mathrm{B}}T)\left[1 - \frac{\lambda p_{\mathrm{F}}}{2k_{\mathrm{B}}T}U\right]U. \tag{3}$$

The first term describes the velocity independent damping coefficient γ responsible for the linear damping force $F_{\mathrm{T}}^{\mathrm{lin}} = \gamma U$ which is the form commonly used in thermometry. The second, velocity dependent term $\beta(U) = \gamma\lambda p_{\mathrm{F}}U/2k_{\mathrm{B}}T$, represents the contribution from Andreev reflection to damping. Since the total damping coefficient $\gamma - \beta(U)$ is related to the linewidth, Δf, the linewidth versus velocity plot measures the contribution from Andreev reflection to the total damping (Fig. 3, left panel). At very low drives Δf is nearly constant, but as the velocity increases, the number of quasiparticles scattered by the Andreev process increases. However, when scattered, they exchange only a tiny amount of their momenta, of the order of $(\Delta/E_{\mathrm{F}})p_{\mathrm{F}}$, where E_{F} is the Fermi energy and, as a result, the damping and the corresponding linewidth Δf decreases. At sufficiently high velocities, Δf begins to increase. The

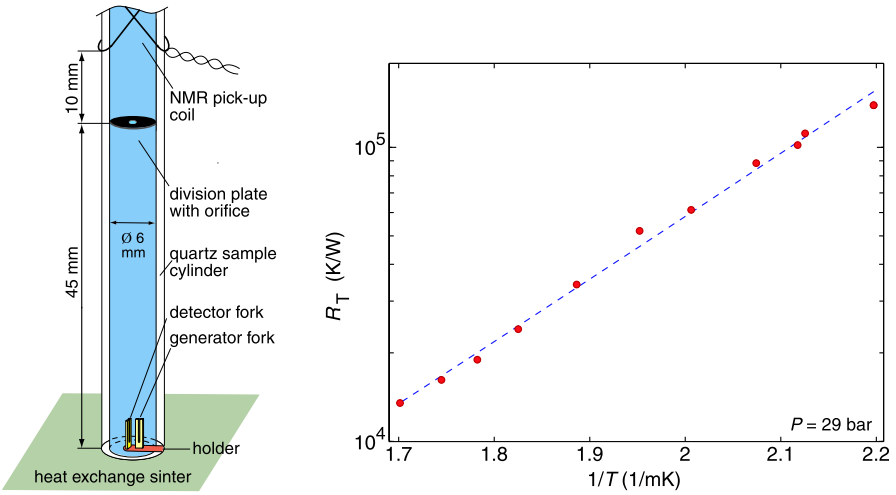

Fig. 4 (Color online) *(Left)* Side view of the two forks in the sample cylinder which is primarily used for NMR measurements [28]. *(Right)* Thermal resistance $R_T = \Delta T/\dot{Q}$ measured in steady state from the temperature rise ΔT of the detector fork while the generator fork is heated at the power level $\dot{Q}$. The *fitted line* corresponds to $R_0 \approx 11$ K/W, when $\Delta = 1.96\, k_B T_c$ is used from Ref. [24]

velocity (~ 1 mm/s) at which this occurs could be called a critical velocity above which the fork's motions produce pairbreaking and/or generate turbulence, as has been explained to be the case for vibrating wires [8, 9].

4.2 Andreev Reflection from Turbulent Vortex Tangle

On the left in Fig. 4 the sample container setup with two tuning forks is shown. The forks are mounted next to each other on a support plate which blocks some of the open cross section of the quartz sample cylinder which is 6 mm in diameter. The end of the quartz tube is located at a distance ~ 2 mm from the sintered heat exchanger surface. When the generator is operated at high drive in the ballistic temperature regime ($k_B T \ll \Delta$), its heat flux $\dot{Q}$ causes a temperature rise ΔT to appear, which is registered with the detector. This is caused by a thermal resistance $R_T = \Delta T/\dot{Q} = R_0\,(k_B T/\Delta)\,\exp(\Delta/k_B T)$, which is dominated by the constriction in the open cross section in the region around the forks. Following the analysis in Ref. [27], the coefficient R_0 can be written in the form $R_0 = 2\pi^2\hbar^3/(p_F^2 \Delta k_B A_h)$. Using the value $\Delta = 1.96\, k_B T_c$, which we take from Ref. [24] and which we use in our temperature calibration of the fork against the NMR signal, then a fit of the $(\Delta T, \dot{Q})$ data in Fig. 4 gives $A_h \approx 3\,\text{mm}^2$ for the effective cross section of the channel in the region around the forks. Since the fork measures primarily the quasiparticle density $\propto \exp(-\Delta/k_B T)$, at higher generator drives the direct contribution from the temperature rise owing to the power consumption $\dot{Q}$ has to be subtracted first, to distinguish finer details.

Figure 5 describes the measurement of Andreev reflection from the vortex tangle produced by the generator fork. This is similar to the Lancaster studies of vibrating

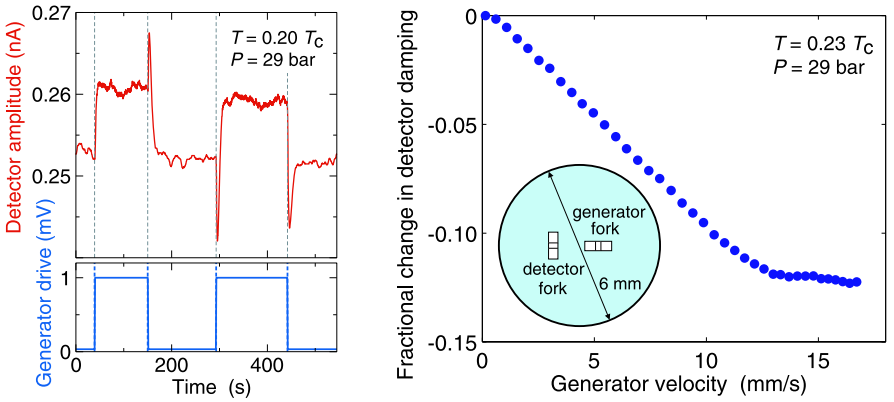

Fig. 5 (Color online) Generation and detection of turbulence in ^{3}He-B using two forks. The generator is driven at different steady drive levels, to generate a turbulent tangle which extends to the detector. The detector is operated at constant low level. The presence of the tangle is observed as a decrease in the damping Δf of the detector (equivalent to an increase of the oscillation amplitude at resonance). *(Left)* Original time trace of the amplitude of the detector fork as the drive of the generator fork is switched between low and high levels. *(Right)* The relative change of the resonance width of the detector versus the oscillation amplitude of the generator, after subtracting for the temperature rise from the thermal resistance R_T. *(Inset)* Top view of the mounting of the two forks in the sample cylinder

wire or vibrating grid generated turbulence [25, 26]. In the left panel the detector response (as measured) is recorded as a function of time when heating pulses are fed to the generator. The detector is driven at low velocity (below 0.5 mm/s), while the square pulses to the generator are at relatively high velocity (5.6 mm/s in the left panel). During the pulse the damping of the detector output decreases, which effectively corresponds to cooling. The apparent cooling happens in spite of the fact that heat is simultaneously added to the system by the generator pulse. The Lancaster interpretation of this bizarre phenomenon is Andreev reflection from the generator-produced vortex tangle which partially surrounds also the detector and screens it from the impinging quasiparticle shower. Since the quasiparticle density around the detector determines its damping Δf, the damping decreases when the screening by the tangle is effective.

The right panel in Fig. 5 shows that with increasing generator velocity the reduction of Δf further increases. Here we plot the relative change in the detector damping, $(\Delta f - \Delta f_0)/\Delta f_0$, where Δf is the measured width of the detector's resonance response and $\Delta f_0(T)$ is its temperature-dependent width in the absence of any screening. Thus the temperature rise from the thermal resistance has been taken into account. The resulting dependence is similar to that measured with vibrating wires in Lancaster [25]: With increasing generator velocity more vortices are produced, the line density in the tangle increases and its spatial extent in volume grows. Both effects increase the screening of the detector and help to extend the cooling to higher generator drives. Qualitatively this result is independent of which fork is used as generator/detector.[4] From the Lancaster measurements it is known that with decreasing

[4]With their roles reversed the slope in the right panel of Fig. 5 becomes $\sim 20\,\%$ steeper.

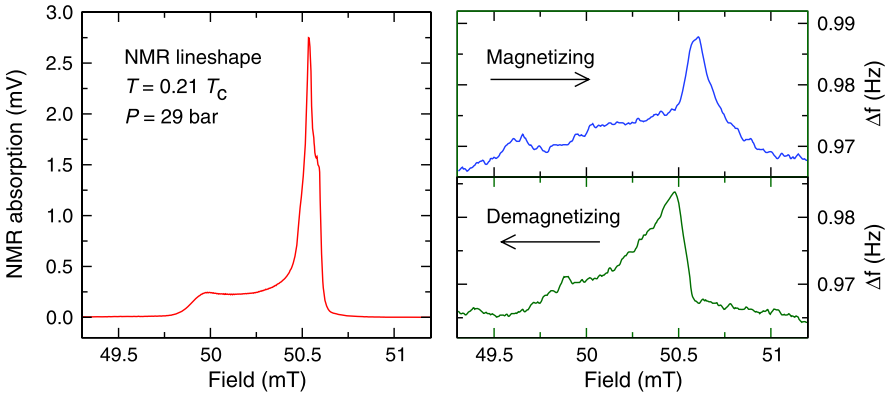

Fig. 6 (Color online) Bolometric detection of NMR resonance absorption with a tuning fork. Quasiparticles created by resonance absorption within the pick-up coil of the setup in Fig. 4 effuse through the orifice and raise the quasiparticle density in the space with the two tuning forks owing to the thermal resistance R_T. *(Left)* The NMR line shape measured with the pick-up coil. *(Right)* The resonance width Δf of the fork recorded (with the detector fork of Fig. 5) for linear upward and downward moving NMR field sweeps (of 100 s duration). The largest differences are caused by the finite thermal time constant for the recovery after a heat pulse

temperature the decreasing slope in Fig. 5 (right panel) becomes steeper, i.e. the apparent cooling becomes stronger. At the lowest generator drives a critical velocity of order ~ 0.5 mm/s might exist, where the screening and the tangle formation start, and which thus would correspond to the critical velocity in the right panel of Fig. 3.

5 Conclusions

The quartz tuning fork is a practical and sensitive multipurpose tool in liquid helium research which can be operated over the entire temperature range from room temperature down to sub-millikelvin temperatures. As a sensor it is usually operated in the linear mode, vibrating at low amplitude with a resonant response which is of Lorentzian shape. In this mode it is useful as pressuremeter, viscometer, secondary thermometer, and bolometer (see the example in Fig. 6 from the sub-millikelvin regime). Both the width of the frequency response and the resonant frequency can be measured and provide information on the fluid density and viscosity [13]. At high drive in the non-linear regime the fork can be used to study cavitation [18] and as a generator of turbulence in both classical and quantum fluids. An advantage is that it can be operated continuously through the superfluid transition, allowing complementary measurements on viscous and superfluid turbulence. By now the fork has been used for turbulence studies with promising results in ^{4}He, ^{3}He, as well as in ^{3}He-^{4}He mixtures [29].

Much of the work with the tuning fork so far has been repetition of earlier measurements with vibrating wire resonators. It is not yet clear how well the tuning fork compares with the most sensitive vibrating wire devices or what will be its value as a primary measuring instrument for detecting vortices and turbulence. The analysis and

evaluation of such measurements is currently pursued by several research groups. If these studies are successful, it would ultimately be desirable to obtain quartz oscillators of much smaller size than the present tuning forks.

Acknowledgements The authors thank a number of colleagues for discussions and for information about their results prior to publication. This work is supported by research plans MS 0021620834, AVOZ 10100520, GAČR under 202/05/0218, GAUK 7953/2007, APVV 51-016604, VEGA 2/6168/06, CE I-2/2007, Academy of Finland (grants 213496, 211507), EU Transnational Access Programme (RITA-CT-2003-505313), and by the U.S. Steel Košice s.r.o.

References

1. E.L. Andronikashvili, J. Phys. USSR **10**, 201 (1946)
2. E.L. Andronikashvili, Zh. Eksp. Teor. Fiz. **18**, 424 (1948)
3. E.L. Andronikashvili, Prog. Low Temp. Phys. **5**, 79 (1967)
4. W.F. Vinen, Proc. R. Soc. A **260**, 218 (1961)
5. M. Morishita et al., J. Low Temp. Phys. **76**, 387 (1989)
6. H. Yano et al., Phys. Rev. B **75**, 012502 (2007)
7. N. Hashimoto et al., Phys. Rev. B **76**, 020504 (2007)
8. S.N. Fisher et al., Phys. Rev. Lett. **63**, 2566 (1989)
9. D.I. Bradley, Phys. Rev. Lett. **84**, 1252 (2000)
10. J. Martikainen et al., J. Low Temp. Phys. **126**, 139 (2002)
11. E.P. Eernisse et al., IEEE Trans. Ultrason. Ferroelectr. Freq. Control **35**, 3230 (1988)
12. K. Karrai, R.D. Grober, Tip-sample distance control for near-field scanning optical microscopes, in *Near-Field Optics*, ed. by M.A. Paesler, P.T. Moyer. Proc. SPIE, vol. 2535 (1995), p. 69; http://www.nano.physik.uni-muenchen.de/publikationen/Preprints/p-00-03_Karrai.pdf
13. R. Blaauwgeers et al., J. Low Temp. Phys. **146**, 537 (2007)
14. D.O. Clubb et al., J. Low Temp. Phys. **136**, 1 (2004)
15. M. Blažková et al., Phys. Rev. E **75**, 025302 (2007)
16. M. Blažková et al., J. Low Temp. Phys. **148**, 305 (2007)
17. H. Schlichting, K. Gersten, *Boundary-Layer Theory* (Springer, 1996)
18. L. Skrbek et al., J. Low Temp. Phys., these proceedings
19. J. Jäger et al., Phys. Rev. Lett. **74**, 566 (1995)
20. M. Niemetz et al., J. Low Temp. Phys. **126**, 287 (2002)
21. M. Niemetz et al., J. Low Temp. Phys. **135**, 447 (2004)
22. D. Charalambous et al., Phys. Rev. E **74**, 036307 (2006)
23. R. Hänninen et al., Phys. Rev. B **75**, 064502 (2007)
24. I.A. Todoshchenko et al., J. Low Temp. Phys. **126**, 1449 (2002)
25. S.N. Fisher et al., Phys. Rev. Lett. **86**, 244 (2001)
26. D.I. Bradley et al., Phys. Rev. Lett. **95**, 035302 (2005)
27. C. Bäuerle et al., Phys. Rev. B **57**, 14381 (1998)
28. A.P. Finne et al., Rep. Prog. Phys. **69**, 3157 (2006)
29. G. Sheshin, J. Low Temp. Phys., these proceedings